The microstructure of polydisperse, charged colloidal suspensions by light and neutron scattering

Norman J. Wagner, Rainer Krause, Adrian R. Rennie, Bruno D'Aguanno, and Jim Goodwin

Citation: The Journal of Chemical Physics **95**, 494 (1991); doi: 10.1063/1.461450
View online: http://dx.doi.org/10.1063/1.461450
View Table of Contents: http://scitation.aip.org/content/aip/journal/jcp/95/1?ver=pdfcov
Published by the AIP Publishing

The microstructure of polydisperse, charged colloidal suspensions by light and neutron scattering

Norman J. Wagner, Rainer Krause,[a] Adrian R. Rennie,[b] Bruno D'Aguanno,[a] and Jim Goodwin[b]
Department of Chemical Engineering University of Delaware, Newark, Delaware 19716

(Received 15 November 1990; accepted 29 March 1991)

Structure measurements of a suspension of charged polystyrene spheres with significant polydispersity (16%) are reported for a wide range of particle and added salt concentrations and scattering wave vector. Small angle neutron scattering yielded the structure factors of concentrated samples that have had extensive rheological characterization. A Schulz model of the particle size distribution was used to reduce the intensity data and as a basis for the theoretical fits of the structure factors. Static light scattering measurements yielded the structure factors of diluted, deionized samples. Dynamic light scattering was also performed to study the relaxation of these structures. These measured structures were fit with a recent theory that accounts for both size and charge polydispersity in the suspension. These results and the previous extensive, rheological investigations and physical characterization yield a complete data set on a well-characterized, model system that can be used to test theories of the statics and dynamics of polydisperse colloidal suspensions.

I. INTRODUCTION

There is a large research effort directed toward understanding the macroscopic behavior of complex fluids in terms of the underlying nature of the fluid's constituents and their fundamental interactions. In particular, colloidal fluids exhibit a wide range of mechanical, optical, and electrical behavior in a multiplicity of practical applications. Consequently, a microscopically based understanding of these fluids is desirable to further the design and development of such materials for specific uses. For example, the development of a colloidal suspension for a ceramic precursor or an electrorheological fluid could benefit substantially from understanding the macroscopic property changes resulting from variations in the fundamental nature of the particles, solvent, and added salt, polymer, and surfactant. Similar arguments are made for the development of superior microemulsions and polymer solutions tailored for specific applications.

Motivated by experimentally based intuitive guidelines that arose from studies of colloidal suspensions and the need to modify these suspensions for specific applications, a more rigorous treatment based in statistical mechanics has been developed.[1-15] The fundamental idea is to treat the suspension as a one-component macrofluid; this stochastic system is then amenable to description by statistical mechanics. Once certain simplifications have been made, such as approximations for many-body effects, then knowledge of the interparticle interactions and the constituents of the system enable complete specification of the equilibrium state of the sample.[15,16] The theory takes as inputs the microscopic variables of the sample and returns the equilibrium structure as characterized by the radial distribution function. Further work relates this structure and the microscopic forces to the mechanical and optical properties of the sample.[1,2,6,10,12,13,15,17] There is certainly more than one way to perform the latter step; the methods include solving a nonequilibrium Smoluchowski equation[1,2,4,10,12,14,15,17] and using a mode-coupling closure to the equations of generalized hydrodynamics.[6,7] Nevertheless, these approaches that relate the macroscopic behavior to the microscopic properties all have as an intermediate the equilibrium structure of the sample. This quantity is fundamental to the development of the theory of these complex fluids.

In the recent past, there have been a number of attempts to test this theoretical development for a model hard-sphere suspension.[9,11,12,17-27] The results of comparing the rheological measurements and equilibrium and nonequilibrium microstructure measurements with the predictions of the theories mentioned above were plagued by the dominant role of hydrodynamic interactions in dense hard-sphere suspensions. The long-range nature of hydrodynamic interactions and their relative importance and coupling to the other interparticle and Brownian forces results in an intractable many-body problem that is yet to be resolved. However, limited simulations using the Stokesian dynamics technique[28,29] have been useful in identifying some problems in the limiting assumptions necessary to solve the theory.

The results of this comparison motivated the examination of suspensions where interparticle forces dominate the behavior. One such model system is that of charged polystyrene latex in water, which is a colloidal suspension stabilized by surface charges on the particles. The range of the Coulomb interactions can be controlled by the addition of salt ions that screen the particles. Thus, it is possible to have significant correlations between particles that are dilute in a hydrodynamic sense and to vary the structure of the suspension independently from the particle concentration. Recent

[a] Fakultät für Physik, Universität Konstanz, Germany.
[b] School of Chemistry, University of Bristol, Bristol BS8 1TS, England.

 0021-9606/91/130494-15$03.00

and previous studies have developed both a description of the interaction forces,[30–32] the microstructure of these suspensions,[16] and the resultant rheology in the limit of linear response.[4–7,10,15,33–36] There have been some limited studies of the microstructure and rheology of these suspensions in the past, but surprisingly few on one, well-characterized sample. Quasielastic light scattering (QELS) studies on most suspensions of rheological interest are impossible because concentrated suspensions are usually strong multiple scatterers. However, small angle neutron scattering (SANS) is not plagued by multiple scattering for these systems and has been used in some previous structural studies.[37,38] To properly test the statistically based theories for the macroscopic behavior of such suspensions, the minimum information required consists of the particle size, polydispersity, shape, charge, added salt concentration, measurements of the equilibrium microstructure, and rheological measurements in the linear response regime. When possible, nonequilibrium microstructure measurements are also very useful in understanding the linear and nonlinear dynamics of the suspension.

In this paper, we report the results of both small angle neutron scattering and static and dynamic light scattering measurements on a suspension of charged latex particles in water, over a wide range of salt and particle concentrations. This well-characterized sample has been the object of detailed rheological measurements—modulus, viscosity, and relaxation spectrum.[39,40] It is our goal to provide the complementary structure measurements to completely characterize the material, which will be used to test the fundamental ideas in the above theories. In the following, the sample and experimental procedure for both SANS and static and dynamic light scattering will be presented. This is followed by the presentation of the resultant structures and a comparison with the best theory available for these systems, which is discussed in light of the applicability of the statistical mechanical theory to adequately describe these model fluids. A detailed comparison of the rheological behavior, these measured structures, and the various theories is forthcoming.

II. STRUCTURE DETERMINATION

The basic aspects of determining the microstructure of a complex fluid are well documented.[41] The scattering of both thermal neutrons and photons can be used to measure the structure, with similar formalisms for reducing the experimental measurements to the material structure in both techniques. Light scattering is limited to dilute suspensions or systems with small refractive index differences as photons are strongly scattered by the electrons in the material. Neutron scattering is less subject to multiple scattering as the nuclear spin coherent interaction of neutrons with the nuclei is small. Colloidal suspensions are nonabsorbing to thermal neutrons ($\lambda \simeq 1$ nm) and the scattering equations parallel the Rayleigh–Gans–Debye theory for light scattering.[42] The combination of the two techniques covers a wide range in wave vector and material parameters.

The elastic scattering of thermal neutrons and the quasielastic scattering of photons yield a direct measure of the structure factor, weighted by the form factor of the scatterer, the absolute scattering length density difference of the scatterers from the solvent, and the number of scatterers. In going from the measured scattering intensity to the quantities of interest, namely structure factor, form factor, scatterer radius, and concentration, there is an experimental methodology enabling one to extract this information directly from a series of measurements. For neutron scattering, this is outlined in the handbook for data analysis at the Institute Laue-Langevin.[43] The procedure reduces the scattering intensity $I(q)$ by corrections for the incoherent, isotropic scattering from the sample geometry and cell, corrections for background, and corrections for the detector geometry. The resulting ratio of this quantity to a reference $R(q)$ is then plotted to abstract any leftover background intensity and to determine a normalization for reduction by the form factor. These measurements also yield the particle radius, concentration, and the scattering density difference of the material from the medium. Given the shape and composition of the scatterers, accurate predictions for the form factors are used to reduce the data further to the structure factors. Thus, with a consistent set of experiments, it is possible to determine completely the quantities mentioned above, requiring only fundamental knowledge of the system composition, which is obtained from independent measurements. Below we reproduce some of the fundamental relations concerning SANS, QELS, and the data reduction, referring the reader to Ref. 41 for more detailed derivations.

The scattering vector $\mathbf{q}$ is given by the difference between the incident and scattered wave vectors in the medium with refractive index n_s as

$$\mathbf{q} = \mathbf{q}_0 - \mathbf{q}_s; \quad q = |\mathbf{q}| = \frac{4n_s\pi}{\lambda}\sin\left(\frac{\theta}{2}\right). \tag{1}$$

The measured scattered intensity $I(q)$ is proportional, to within an instrument factor (which will be set to one), to the structure of the material as

$$I(q) = S(q)\overline{F}_s^2(q) + \overline{F_s^2(q)} - \overline{F}_s^2(q), \tag{2}$$

where the single particle form function is given by

$$F_s(\mathbf{q}) = \int_{V_p} [\rho_p(\mathbf{r}) - \rho_m(\mathbf{r})]e^{-i\mathbf{q}\cdot\mathbf{r}}d\mathbf{r}. \tag{3}$$

The overbar denotes an average over the scattering volume with V_p the particle volume and $\rho_{p,m}$ the neutron scattering length densities for the particles and suspending medium. For particles of uniform composition, this reduces to

$$F_s(\mathbf{q}) = (\rho_p - \rho_m)\int_{V_p} e^{-i\mathbf{q}\cdot\mathbf{r}}d\mathbf{r}. \tag{4}$$

The structure factor $S(q)$ for the N scatterers is defined as

$$S(q) = 1 + \frac{1}{N}\left\langle \sum_{j\neq k}^{N} e^{i\mathbf{q}\cdot(\mathbf{R}_j - \mathbf{R}_k)} \right\rangle, \tag{5}$$

which is the Fourier transform of the radial distribution function

$$S(q) = 1 + n\int [g(r) - 1]e^{-i\mathbf{q}\cdot\mathbf{r}}d\mathbf{r}, \tag{6}$$

with n the particle number density.

For monodisperse spheres, Eq. (2) reduces to the commonly quoted expression

$$I(q) = S(q)F_s^2(q). \tag{7}$$

In direct analogy, the effective structure factor of a polydisperse system is defined as

$$I(q) = S_{\text{eff}}(q)\,\overline{F_s^2(q)} = S_{\text{eff}}(q)n(\rho_p - \rho_m)^2 V_p^2 P(q), \tag{8}$$

where V_p is the particle volume formed from $\bar{a}$, the mean particle radius, as $V_p = 4\pi[(\bar{a})^3/3]$. Note that the volume fraction is defined in terms of the third moment of the size distribution as $\phi = n4\pi(\langle a^3\rangle/3)$. In Eq. (8) above, the form factor $P(q)$ is defined as

$$P(q) = \sum_i x_i \left(\frac{a_i}{\bar{a}}\right)^6 P_0(qa_i), \tag{9}$$

where x_i is the number fraction of species i and with

$$P_0(qa) = \left[\frac{3(\sin qa - qa\cos qa)}{(qa)^3}\right]^2 \tag{10}$$

the single sphere form factor. This simple form for the intensity results in a complicated function for the effective structure factor

$$S_{\text{eff}}(q) = \frac{1}{\overline{F_s^2(q)}} \sum_\alpha \sum_\beta F_{s,\alpha}(q)F_{s,\beta}(q)S_{\alpha,\beta}(q) \tag{11}$$

as a mixture of both single particle scattering and pair correlation contributions. The subscripts α and β refer to particle species. The partial structure factors are defined as

$$S_{\alpha,\beta}(q) = \frac{1}{N}\left\langle \sum_{i=1}^{N_\alpha} \sum_{j=1}^{N_\beta} e^{i\mathbf{q}\cdot(\mathbf{R}_i^\alpha - \mathbf{R}_j^\beta)} \right\rangle. \tag{12}$$

Because it is easier to reduce the data in terms of the effective structure factor $S_{\text{eff}}(q)$, our results are analyzed according to Eq. (8). In a recent study,[16] it is shown how $S(q)$ can be theoretically determined and how $S_{\text{eff}}(q)$ can be physically interpreted. In what follows, we drop the subscript on $S(q)$ unless necessary, with the understanding that we are analyzing the data in terms of Eq. (8).

The normalized scattering ratio $R(q)$ written for spherical scatterers in a liquid is the ratio of the scattered intensity to that of some reference I_0 (usually water for SANS and toluene for QELS) as

$$R(q) = [n(\rho_p - \rho_m)^2 V_p^2 P(q)S(q) + B]I_0^{-1}, \tag{13}$$

where B is the background scattering. Plotting $R(q)q^4$ against q^4 for large $q\bar{a}$ gives a measure of the incoherent background as the slope and a measure of the prefactor as the intercept. This Porod plot is based on the limiting behavior as $qa \to \infty$ that $S(q) \to 1$ and $P(q) \propto q^{-4}$. Then the intercept has the dependence

$$\lim_{q\to\infty} R(q)q^4 = B_{\text{Porod}} nV_p + A_{\text{Porod}} q^4 \propto n(\rho_p - \rho_m)^2 V_p^2 + \vartheta(q^4). \tag{14}$$

A plot of the intercepts against number density n or volume fraction should be linear with zero intercept and slope proportional to the scattering density and particle volume. As will be shown, the proportionality can be estimated, enabling a consistency check of these quantities. The value of the slope A_{Porod} is to be subtracted from the experimental $R(q)$ values to correct for any leftover background contribution to the scattering. The intercept values are then used to divide out the form factor with the correct weighting.

Another useful analysis is to make a Guinier plot[44] of $\ln R(q)$ vs q^2. In the Guinier limit where the particle correlations are negligible ($qr_g \ll 1$), the scattering ratio becomes

$$\ln[R(q)] = \ln[n(\rho_p - \rho_m)^2 V_p^2] - \frac{(qr_g)^2}{3} = B_{\text{Guinier}} - A_{\text{Guinier}} q^2, \tag{15}$$

where r_g is the radius of gyration. For a homogeneous sphere, the radius of gyration is simply related to the sphere radius a as

$$r_g = a\sqrt{\frac{3}{5}}. \tag{16}$$

Thus, the slope of the Guinier plot is equal to $a^2/5$ and the intercept value $R(q=0) = n(\rho_p - \rho_m)^2 V_p^2$ gives a measure of the scattering density if the number density is known, or vice versa.

Once these plots are made, all of the physical quantities needed to reduce the intensities to structure factors are known. What is needed is a model for the form factor $P(q)$. The use of a dilute, noninteracting sample to provide $P(q)$ is plagued with large error bars due to the low coherent scattering intensity relative to the incoherent background in SANS. A better procedure, and that adopted here, is to measure a number of dilute samples [$S(q) = 1$], fit them to a model form factor, and then divide the scattering ratios by this fit. The Porod plot results are used to normalize the data for SANS. For light scattering where the scattering vector is more limited in extent, the reduced structure is normalized to approach one for the largest q values.

For homogeneous spheres, the particle form factor as defined above in Eq. (8) can be written as a sum over both polydispersity in size and in wavelength as

$$P(\overline{qa}) = \sum_\lambda \sum_i x_\lambda x_i \left(\frac{a_i}{\bar{a}}\right)^6 P_0(q_\lambda a_i), \tag{17}$$

with x_i the number fraction of species i with radius a_i, and x_λ the number fraction of neutrons with wavelength λ. The polydispersity of our sample is known from previous transmission electron microscopy (TEM) measurements and is given in Fig. 1, where the mean radius is 37.8 ± 5.5 nm.[39] There can be some uncertainty in the TEM values as the sample must be dried. Further, interpreting effective diameters of polydisperse samples is not straightforward as neutron scattering measurements give a different moment of the size distribution. We choose to allow this as an adjustable fit parameter to be determined by comparing the model form factor with the dilute scattering measurements.

The polydispersity of the neutron beam has been measured[45] and is nearly a triangular distribution at $\bar{\lambda} = 1.0$ nm with a full width at half-maximum of 9%. This is modeled as a three component mixture with 50% of the intensity distributed evenly about the main peak at the values $\pm 4.5\%$ vari-

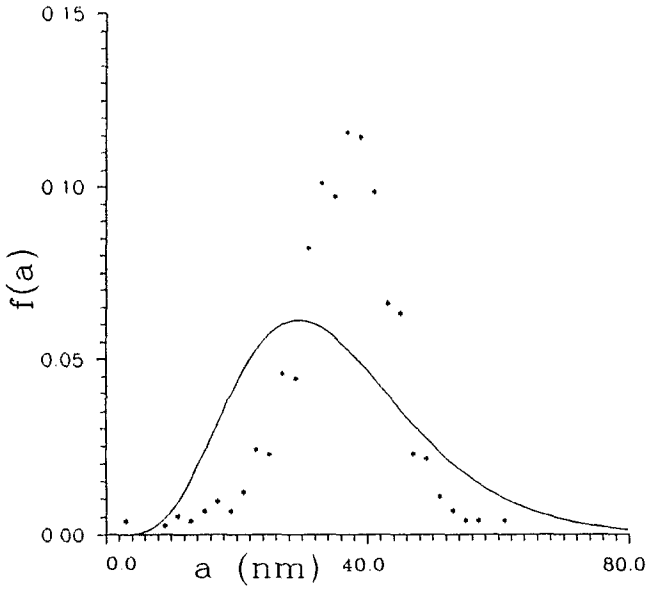

FIG. 1. Particle size distribution as a function of average radius. (*) TEM analysis (Ref. 39); (—) Schulz distribution.

ation in λ. This correction is rather small in comparison with the broad polydispersity of the particles and is almost negligible.

The procedure to construct the form factor is to adjust the mean radius of the distribution to optimize the fit to the measured scattering intensity ratio (minus the background from the Porod plot) for a dilute, noninteracting sample. This constructed form factor is then also fit to a Porod plot and the intercept B extracted. Finally, the value of the structure factor (effective) can be determined by

$$S(q) = \frac{R(q) - A_{\text{Porod}}}{B_{\text{Porod}}} \left[\frac{B_{\text{Porod}}}{P(q)}\right]_{\text{model}}. \tag{18}$$

A. Schulz distribution

An alternative method to model size polydispersity is to fit the data to an analytic function for the size distribution. A commonly used model for a particle size distribution that is continuous and normalized is the Schulz distribution (see Ref. 41). Defining $f(a)$ as the normalized probability of occurrence of particles of radius a,

$$f(a) = (z+1)^{z+1} x^z \frac{\exp^{-(z+1)x}}{\bar{a}\Gamma(z+1)}, \tag{19}$$

where $\bar{a}$ is the mean particle size and $x = a/\bar{a}$, $z = (1-s^2)/s^2$, and $s = \sigma/\bar{a}$ with σ^2 the variance. The line in Fig. 1 is the Schulz distribution determined from the SANS data for the particles used in this study.

Using this distribution for spherical, homogeneous scatterers, an analytical expression has been derived for the form factor[41]

$$P(y) = \frac{9}{2z_1 y^6}\left\{z_1\left[1 - \frac{\cos z_1 w}{(1+4u^2)^{z_1/2}} - \frac{2y \sin z_2 w}{(1+4u^2)^{z_2/2}}\right] + y^2 z_2\left[1 + \frac{\cos z_3 w}{(1+4u^2)^{z_3/2}}\right]\right\}. \tag{20}$$

Here, $u = y/z_1$, $v = \arctan(u)$, $w = \arctan(2u)$, and $z_j = z + j$.

The Guinier analysis can also be modified for polydispersity effects by summing the individual scatterer result given above in Eq. (15) over the Schulz size distribution. The result is

$$R(q) = \left[N(\rho_p - \rho_m)^2\left(\frac{4\pi}{3}\right)^2\right]\int da\, f(a) a^6 e^{-(qa)^2/5}. \tag{21}$$

From this it is readily seen that the intercept B_{Guinier} obtained from the polydisperse equation is simply related to that from the monodisperse equation (15) by

$$B^{\text{poly}}_{\text{Guinier}} = \frac{\langle a^6\rangle}{\langle a\rangle^6} B^{\text{mono}}_{\text{Guinier}} = \langle x^6\rangle B^{\text{mono}}_{\text{Guinier}}, \tag{22}$$

where the normalized nth moment is

$$\langle x^n\rangle = \frac{\langle a^n\rangle}{\langle a\rangle^n} = \frac{\Pi_{j=2}^{n} z_j}{z_1^{n-1}}. \tag{23}$$

Further, expanding the exponential in Eq. (21) above for spherical particles shows that the radius determined by a Guinier plot [Eq. (15)] is

$$A_{\text{Guinier}} = \frac{1}{5}\frac{\langle a^8\rangle}{\langle a^6\rangle} = \frac{1}{5}\frac{\langle x^8\rangle}{\langle x^6\rangle}\langle a\rangle^2. \tag{24}$$

B. Dynamics

The dynamic light scattering (DLS) experiments have been performed in the homodyne mode. The normalized field autocorrelation function

$$g^{(1)}(q,t) = \frac{\langle E(\mathbf{q},0)E^*(\mathbf{q},t)\rangle}{\langle |E(\mathbf{q},0)|^2\rangle} = \frac{S(q,t)}{S(q)} \tag{25}$$

was determined from the intensity autocorrelation function by using the Siegert relation.[46] The dynamic structure factor of the macroion correlations is

$$S(q,t) = \frac{1}{N}\sum_{i,j=1}^{N}\langle e^{\{i\mathbf{q}\cdot[\mathbf{R}_i(t) - \mathbf{R}_j(0)]\}}\rangle. \tag{26}$$

In analyzing DLS data, the cumulant expansion has been widely used. According to Ackerson,[47,48] the first cumulant for a monodisperse sample is

$$K_1(q) = -\frac{d}{dt}\ln g^{(1)}(q,t)|_{t=0} = q^2\frac{H(q)}{S(q)}. \tag{27}$$

The function $H(q)$ contains the effects of the hydrodynamic interaction between the macroions, mediated by the solvent. For systems with negligible hydrodynamic interaction, $H(q)$ reduces to D^0, where

$$D^0 = \frac{k_B T}{6\pi\eta a} \tag{28}$$

denotes the Stokes diffusion coefficient and η is the shear viscosity of the solvent.

III. EXPERIMENT

A. SANS

The measurements reported here were performed on the D11 instrument at the Institute Laue-Langevin in Grenoble, France. The samples of polystyrene latex in water, with controlled salt concentration, were synthesized at the University of Bristol and have had extensive rheological

characterization.[39,40] Four original samples (1C, 2C, 3C, and 4A) were obtained with the given characteristics in Table I, all being of the same batch of colloid, but varying in concentration of colloid and added salt. As indicated, some samples were dialyzed against a known salt concentration, while sample 3C was suspended in a known salt solution. Two of these samples were diluted with distilled water with the appropriate salt concentration and further dialyzed until equilibrated with a salt bath at 25 °C, resulting in two sets of varying particle concentration (1A–1C and 2A–2C). Sample 4A2 is a repeat of sample 4A, used to check reproducibility, and samples B2a and B2b are dilute samples used to determine the form factor. We note that samples 1A, 1B, 2A, and 2B were observed to be liquidlike, while samples 1C, 2C, 3C, and 4A exhibited varying degrees of viscoelasticity, such that 3C and 4A required heating to load into the sample cells. The samples were contained in Helma 1 mm quartz cells. To complete the experimental data set, measurements were made on a blank cell, a cell with pure distilled water, and a cadmium blank.

In order to cover a wide range of scattering vector (10^{-2}–1 nm^{-1}) with good collimation, three sample detector distances were used as follows: 1.5 m with 5 m collimation, 5 m with 20 m collimation, and 20 m with 40 m collimation. The samples were thermostated to 25 °C. Transmissions were measured on every sample at 20 m and plotted against sample volume fraction in Fig. 2. The results should vary approximately linearly with the logarithm of the volume fraction, as observed, with deviations attributable to differences in the sample cells and the experimental geometry for the different measurements.

In scattering, the concentrated samples yielded distinct maximum rings of scattering intensity on the detector, which were sharp and clearly isotropic, except for sample 2C, which showed some evidence of weak Bragg peaks on the intensity maximum (as shown in Fig. 3). The resulting sets of data were then initially reduced at the Grenoble facility, following the documented procedure.[49] Masking corrected for the geometry of the detector and any anomalous detector signals. The masked raw data are first radially averaged about the beam center. Each data set (at the varying sample distances and collimation) is then reduced by subtracting off the incoherent scattering from the cell and the background scattering from the instrument. This is then divided by the similarly corrected water sample. The final ratio is then scaled to the known value for water, so as to be in relative units. After treating the three sets of files in this manner, they were fitted together to correct for any differences in intensities due to collimation effects.

B. Static and dynamic QELS

The light scattering apparatus (ALV, FRG) employed in this study consisted of a computer controlled goniometer table with focusing and detector optics and a power stabilized 3 W argon laser (Spectra Physics), a 4 bit real-time correlator (1023 channels), a digital rate meter, and a temperature control which stabilized the temperature of the sample cell at $T = (21 \pm 1)$ °C. Measurements and data acquisition were controlled by a personal computer. Intensity data were corrected by the dark rate of the photomultiplier and by the angle dependence of the scattering volume. The scattered intensity was measured in steps of 2°. The magnitude of the scattering vector ranged from 0.3×10^{-2} to 3.3×10^{-2} nm^{-1} with the vacuum wavelength of the incident light $\lambda_0 = 488$ nm in aqueous solutions with a medium refractive index $n_s = 1.33$. The beam was focused through an index match fluid (silicon oil) and the scattering cell onto the scattering volume. For scattering cells, we used quartz tubes of 10 mm outer diameter. All measurements were normalized to a reference sample (toluene) in the total q region. The salt-free samples listed in Table I were diluted from a

TABLE I. Sample characteristics. (A) SANS samples; (B) QELS samples.

System	ϕ	C_{salt} (mM)	Preparation	ϕ (Dry weight)
(A)				
1A	0.181	1.0 NaCl	Dialyzed	0.182
1B	0.10	1.0 NaCl	Dialyzed	0.106
1C	0.208	1.0 NaCl	Dialyzed	
2A	0.05	0.1 LiCl	Dialyzed	0.053
2B	0.092	0.1 LiCl	Dialyzed	0.089
2C	0.119	0.1 LiCl	Dialyzed	
3C	0.285	0.01 LiCl	Added	
4A	0.353	10.0 NaCl	Dialyzed	
4A2	0.353	10.0 NaCl	Dialyzed	
B2b	0.001	0.1 LiCl	Added	
B2a	0.01	1.0 LiCl	Added	
(B)				
W1	0.001 25%		Ion exchanged	
W2	0.0125%		Ion exchanged	
W3	0.025%		Ion exchanged	
W4	0.000 625%		Ion exchanged	
W5	0.05%		Ion exchanged	
W6	0.075%		Ion exchanged	
W7	0.10%		Ion exchanged	
W8	0.15%		Ion exchanged	

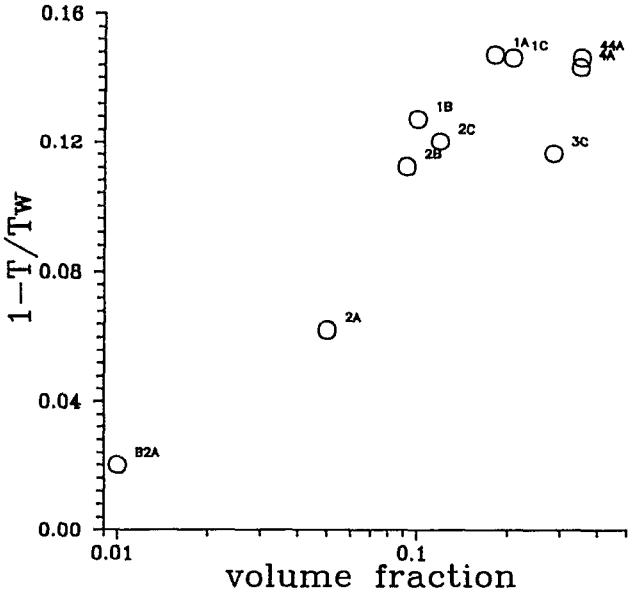

FIG. 2. One minus the SANS transmission measurements normalized to water ($1 - T$) plotted vs the log of the particle volume fraction.

highly concentrated polystyrene latex solution (SANS sample 2C) with deionized water. To minimize the ionic strength of the suspensions, a cleaned, mixed-bed ion exchange resin was added to the samples, removing all the residual salt ions and leaving only the counterions from the colloids and the H^+ and OH^- from water dissociation. The size of the latex was determined from DLS in very diluted monodisperse solutions by applying the cumulant method. The standard deviation of the particle radius was obtained as the ratio of the first two cumulants $\sigma = K_2/K_1^2$.

The DLS data were also analyzed by fitting to a double exponential form as

$$\frac{S(q,t)}{S(q)} = a(q)e^{-[t/\tau_1(q)]} + [1 - a(q)]e^{-[t/\tau_2(q)]}, \quad (29)$$

which is a hypothesis based on a viscoelastic approximation to the dynamics of Brownian suspensions.[7] The relaxation times $\tau_1(q)$ and $\tau_2(q)$, and weighting parameter $a(q)$ can be used to study the linear response of the material to deformation. The fit was performed by a standard nonlinear error minimization algorithm.[50] The first and second cumulants are readily obtained in terms of the three fit parameters τ_1, τ_2, and a as

$$K_1(q) = \frac{a(q)}{\tau_1(q)} + \frac{[1 - a(q)]}{\tau_2(q)},$$
$$K_2(q) = K_1^2(q) - \frac{a(q)}{\tau_1^2(q)} - \frac{[1 - a(q)]}{\tau_2^2(q)}. \quad (30)$$

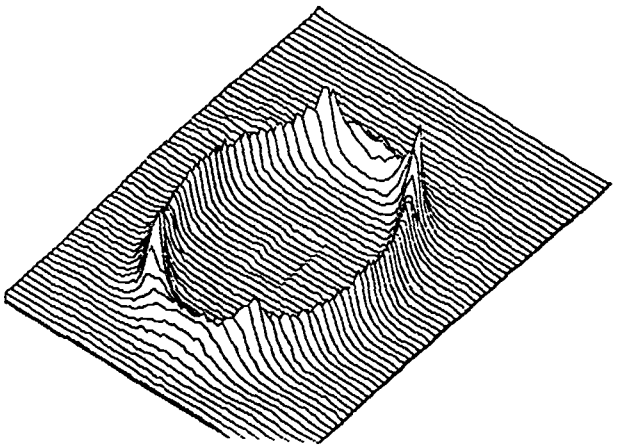

FIG. 3. SANS D11 detector output for sample 2C at distance 5 m.

C. Monte Carlo fits

Monte Carlo (MC) computer simulations of dilute, monodisperse suspensions within the framework of the one-component macroion fluid model were used to fit the QELS structure measurements. The simulations are for monodisperse suspensions interacting via a Yukawa type potential.

$$\beta U(R) = \infty, \quad r < 2a$$
$$= \frac{Q^2 L_B e^{2\kappa a}}{(1 + \kappa a)^2} \frac{e^{-\kappa r}}{r}, \quad r > 2a, \quad (31)$$

with $\kappa = (4\pi L_B nQ)^{1/2}$ the inverse Debye–Hückel screening length, $L_B = e^2/(4\pi\epsilon\epsilon_0 k_B T)$ the Bjerrum length, and Q the charge on the colloids.

A number N particles with diameter $2a$ are placed in a basic cubic cell of volume $V = L^3$ with

$$L = \left[\frac{\pi(2a)^3 N}{6\phi}\right]^{1/3}. \quad (32)$$

Periodic boundary conditions are used. Since $L \sim N^{1/3}$, the number N has to be chosen sufficiently large so that L is greater than the effective range of the pair potential. In all our MC calculations, $N = 256$. The simulations were started from a face-centered-cubic (fcc) lattice configuration or from a configuration obtained from a previous computation. Sufficient computational MC steps were allowed for the system to reach thermal equilibrium, using the usual Metropolis algorithm.[51,52] The radial distribution function $g(r)$ was calculated and the static structure factor $S(q)$ determined by numerical Fourier transformation. The effective charge on the colloidal particles and the concentration were adjusted for each sample so that the peak height and position of the main peak in $S(q)$ agreed with the static light scattering measurements.

IV. RESULTS AND DISCUSSION

A. Form factor determination

The form factor was calculated by both the analytic Schulz result, Eq. (20), and the discrete summation over the TEM distribution, as given in Eq. (17). In using the Schulz distribution, both the mean particle radius and the standard deviation of the sample were determined by the fit to the dilute measurements B2a and B2b. A least-mean-square fit procedure resulted in the values of $\bar{a} = 35.0$ nm and $s/\bar{a} = 0.16$ as the best fit. These are shown in Figs. 4(a) and 4(b). No account of the polydispersity in neutron wavelengths was explicitly made. However, for such a small dis-

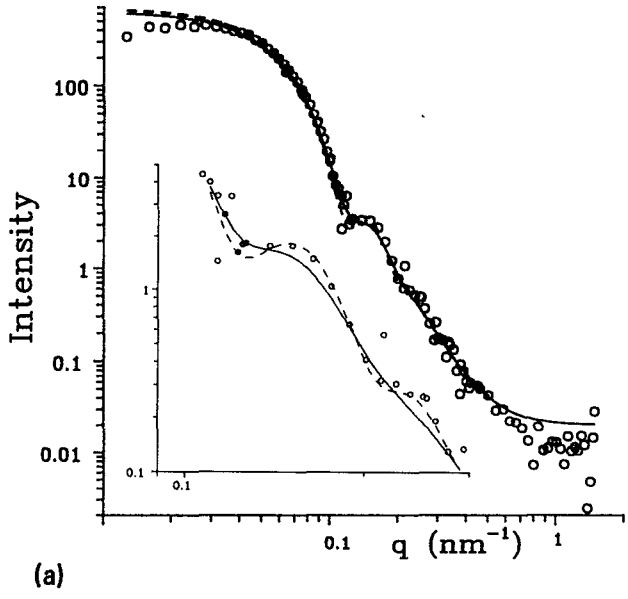

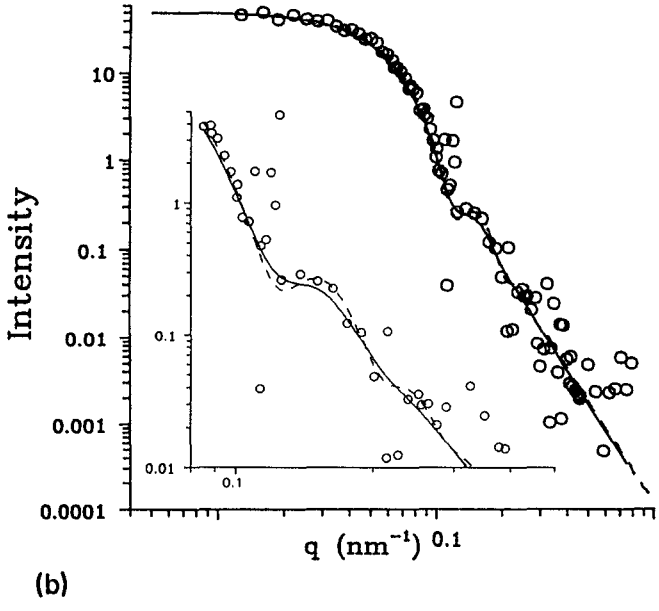

FIG. 4. (a) B2a SANS $R(q)$. (O), (—) Schulz distribution fit; (- - -) TEM based distribution fit. (b) B2b, the same as above. The insets show the detail around the first minimum.

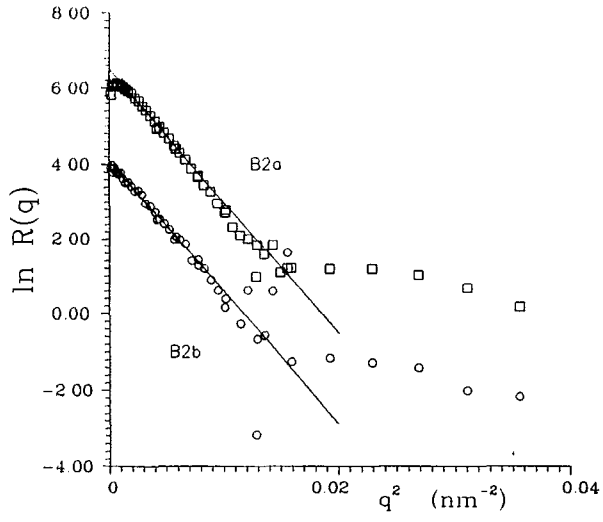

FIG. 5. Guinier plots of ln $R(q)$ vs q^2 for samples B2a and B2b; (-) best fit lines.

persion relative to the dispersion in particle sizes, these effects are included together in the effective variance of the fit. A variation of $\pm$ 1.0 nm in the mean size and $\pm$ 0.02 in $s/\bar{a}$ made a noticeable difference in the quality of the fit.

For the form factor derived from Eq. 17, the value of $\bar{a}$ was allowed to float and the entire distribution shifted proportionally to match this value. The value of $\bar{a} = 42.0$ nm was again determined by a least-square fit. Figures 4(a) and 4(b) compare these two fits, with the noticeable difference that the Schulz distribution results in less pronounced minima in the form factor (see the inserts).

In Fig. 5, the data were plotted as ln $R(q)$ vs q^2 to extract the Guinier radius (Table II). The plots have a linear region at low qa and can be fit by a straight line, where the low qa data that show the influence of interparticle structure in sample B2a were rejected from the fit. The results for the particle radius (Table III), extracted from Eq. (15), are in good agreement with one another, but significantly (27%) higher than that determined by TEM.[39] By using the value of the polydispersity obtained from the Schulz fit, both the po-

TABLE II. Porod and Guinier plot results.

System	ϕ	Porod plot		Guinier plot	
		$A \times 10^5$	B	$A \times 10^{-5}$	B
1A	0.181	0.390 ± 0.008	0.0923 ± 0.0449	0.385 ± 0.073	6.25 ± 0.12
1B	0.10	0.219 ± 0.008	0.0830 ± 0.0425	0.713 ± 0.080	6.29 ± 0.13
1C	0.208	0.472 ± 0.010	0.127 ± 0.0531	0.197 ± 0.087	6.11 ± 0.14
2A	0.05	0.0938 ± 0.0064	0.0494 ± 0.0360	0.614 ± 0.072	6.45 ± 0.11
2B	0.092	0.180 ± 0.007	0.0518 ± 0.0403	0.962 ± 0.080	5.85 ± 0.13
2C	0.119	0.253 ± 0.008	0.0478 ± 0.0795	0.635 ± 0.085	5.71 ± 0.14
3C	0.285	0.697 ± 0.144	0.0142 ± 0.0698	− 0.112 ± 0.088	6.48 ± 0.14
4A	0.353	0.702 ± 0.2390	0.440 ± 0.0960	0.311 ± 0.088	6.31 ± 0.14
4A2	0.353	0.726 ± 0.189	0.360 ± 0.0860	0.0557 ± 0.088	6.25 ± 0.14
B2b	0.001	0.000 997 ± 0.000 10	0.0076 ± 0.0108	− 0.327 ± 0.115	4.03 ± 0.18
B2a	0.01	0.0135 ± 0.0006	0.0198 ± 0.0115	− 0.352 ± 0.016	6.50 ± 0.059

TABLE III. Radius from Guinier plots.

System	Radius (nm)	
	Monodisperse	Polydisperse
B2b	41.7 ± 2.5	35.8 ± 2.2
B2a	41.9 ± 1.9	35.9 ± 1.6
Schulz form factor	40.9 ± 1.8	35.1 ± 1.5
TEM form factor	41.0 ± 1.8	35.1 ± 1.5

lydisperse Guinier equation (21) or the equivalent conversion equation (24) result in excellent agreement for the radius, as listed in Table III. Applying the same analysis to the model Schulz form factor demonstrates the consistency of this technique for handling polydispersity (see Table III).

Dynamic light scattering was performed on highly diluted samples where particle correlations were negligible. The results of using the cumulant method to determine the particle radius and polydispersity are $a \pm da = 39.6 \pm 7.6$ nm, with a standard deviation of 19%. This technique is sensitive to the hydrodynamic radius of the sample, so the close agreement with the above analysis indicates that the particles are physically spherical and are not aggregated.

B. Volume fraction and scattering length density

The scattering density difference for the samples was extracted from the intercept values of the Guinier plot. From Eq. (15), it is seen that the intercept of the Guinier plot B_{Guinier} is equal to

$$B_{\text{Guinier}} = \ln R(q=0) = n(\rho_p - \rho_m)^2 V_p^2 = \frac{\phi}{\langle x^3 \rangle}(\rho_p - \rho_m)^2 V_p. \quad (33)$$

The results, based on using the known volume fraction and the particle radius determined by the monodisperse Guinier analysis are shown in Table IV. The value of -0.56×10^{-10} cm^{-2} was used for the medium (water) and the accepted value for polystyrene is 1.41×10^{-10} cm^{-2}. Using the polydisperse Guinier fit or the conversion equation (22) results in an improvement of the values (see Table IV). The results are still low, which could be due to a number of factors that include error in the known volume fraction. However, the Porod plot that follows shows that this error is negligible.

Table II summarizes the results for the slope (background) and intercept values obtained from Porod plots of each sample. These values were subtracted off the scattering ratios and used for normalization of the structure factors,

TABLE IV. Scattering length density.

System	$\rho_{\text{polystyrene}}$ (10^{-10} cm^{-2})	
	Monodisperse	Polydisperse
B2b	0.89 ± 0.05	1.19 ± 0.06
B2a	0.97 ± 0.04	1.27 ± 0.05
Porod data (5 m)	1.34	
Porod data (1.5 m)	1.28	

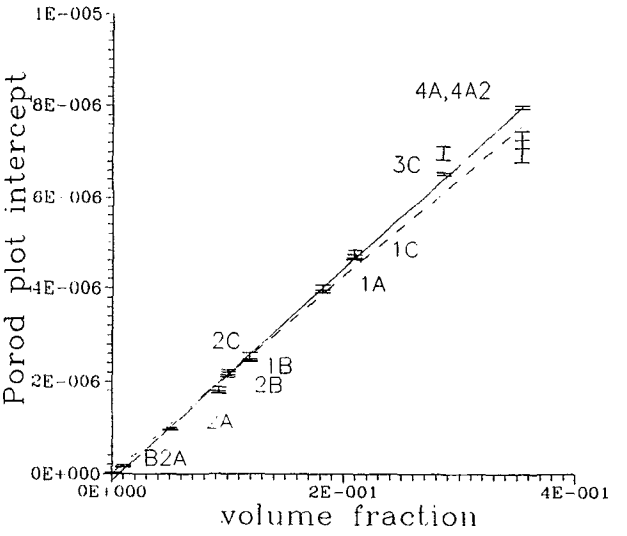

FIG. 6. Porod plot for the SANS data 1.5 m (—) best fit line; 5 m (- - -) best fit line.

respectively. The intercepts of the Porod plots are plotted against volume fraction in Fig. 6 for the 1.5 and 5 m data. Excellent agreement with the expected volume fraction is evident by the linearity of the plots. The measured background has a general trend to increase with volume fraction, although these values do not appear to be that systematic or significant.

As mentioned above, the slopes of the lines of the Porod plot intercepts against expected volume fraction can be used to estimate the scattering length density difference. From Eq. (14) above, this slope is seen to be proportional to the particle volume fraction times the square of the scattering length density difference, times some constant that gives the decay of $P(q)$ in the q^{-4} regime. This decay coefficient is estimated by averaging the single particle form factor over a cycle of 2π. The error in doing this is expected to be of order $1/qa$ and thus, should be small for our data. The slope in the plots of Fig. 6, denoted by A_P, is then

$$A_P \approx \frac{V_p}{\langle x^3 \rangle}(\rho_p - \rho_m)^2 \frac{1}{2\pi}\left[\int_0^{2\pi} \sin^2\theta \, d\theta + O\left(\frac{1}{qa}\right)\right]. \quad (34)$$

The results of this calculation, listed in Table IV, are in reasonable agreement with the accepted value of 1.41×10^{-10} cm^{-2} when 35 nm is taken for the particle radius.

C. Theoretical fits of the structure factor

A successful model for the structure factor of polydisperse, charged suspensions of spherical particles has been verified[16] and previously used in the determination of transport coefficients.[15] It is based on solving the Ornstein–Zernike equation[53] with the Rogers and Young[54] closure (RY). This essentially blends the Percus–Yevick (PY) and hypernetted chain (HNC) closures into a thermodynamically self-consistent integral equation for the structure. The result

is constrained to satisfy equal osmotic compressibilities calculated from both the pressure equation and the Ornstein–Zernike route. Polydispersity is modeled by an n component discretization of the Schulz distribution, requiring the first n moments of the discretized distribution to equal the corresponding moments for the continuous Schulz distribution. Charge polydispersity is assumed to scale as the surface area of the particle, i.e., a constant surface charge density.

For a given interparticle potential, the OZ equation with the RY closure and the condition of thermodynamic consistency constitute a closed set of equations for the microstructure of the liquid phase. An n component system has $n(n+1)/2$-independent radial distribution functions characterizing the mixture, requiring simultaneous solution of an equal number of coupled OZ–RY equations. The equations are solved for a choice of RY mixing parameter, the degree of thermodynamic consistency calculated, and a new value for the mixing parameter is estimated to improve the consistency. This iteration procedure is continued until an acceptable degree of consistency is achieved. For polydisperse systems requiring a large number of components, the computational time requirements for solving the coupled integral equation matrix, necessary at every iteration, become prohibitive. Further, systems with strong correlations and high particle density require finer resolution in the numerical calculations for mathematical accuracy and convergence in solving the equation matrix. Hence, our SANS samples, which require a five component discretization and have a high volume fraction, cannot be modeled by the full OZ–RY scheme given the present computational limitations. The full OZ–HNC equations (essentially one iteration with the RY mixing parameter set to infinity) are tractable and can be used for the fitting.[16] The QELS samples have a significantly longer screening length and so polydispersity effects on the microstructure are reduced. Here a three component fit, for which the RY scheme is computationally tractable, suffices to accurately model the distribution.

The interparticle potential is modeled as a Yukawa potential, or equivalently, the Debye–Hückel approximation to the linearized Poisson–Boltzmann equation. Essentially, this results in two fit parameters for the systems of interest here, the charge on the colloid and the screening length [see Eq. (31)]. The screening length is given in terms of the ionic strength, which depends on the total concentration of all small ions. For the samples dialyzed against a known salt bath, the ionic strength in the suspension can be estimated as a starting point for the fitting procedure from considering the Donnan equilibrium across the dialysis membrane.[55] Equating the chemical potentials of the salt in the colloidal suspension and the dialysis bath and accounting for electroneutrality yields an equation for the salt concentration in the suspension C_{salt} in terms of the charge and volume fraction of the colloids (Q and ϕ), the salt concentration in the dialysis bath (C_{dialysis}), and the activity coefficients. Assuming ideal mixing then gives[40]

$$C_{\text{salt}} = -\left(\frac{QC_{\text{particles}}}{2}\right) + \frac{1}{2}\left[(QC_{\text{particles}})^2 + 4C_{\text{dialysis}}^2(1-\phi)^2\right]^{1/2}. \quad (35)$$

These values lead to estimates for the salt concentrations that are about one-half of the bath concentrations for the colloidal suspensions considered here. For the QELS samples in equilibrium with ion exchange resin, where the only appreciable counterion concentration is from dissociated ions, the fit reduces to just the effective charge. In practice, slight adjustments in the particle concentration are also made to improve the fit of the peak position. This adjustment is kept within the experimental uncertainty in the volume fraction.

The fitting procedure uses the mean particle radius (35 nm) and the polydispersity (16%) fixed by the form factor fit. The number of size components is set and the distribution discretized. The OZ–RY equation matrix is then solved for the given values of colloid charge, added salt concentration, and colloid concentration. Small adjustments in the latter parameter are made to fit the position of the primary peak in $S(q)$ to the experimental measurements, if necessary. Iterations on the values of Q and C_{salt} (where applicable) are performed until an optimal fit of the data is achieved. As the SANS samples require a minimum of five components in the size distribution to capture accurately the structure, the simpler OZ–HNC equation matrix was solved. The results of this fitting procedure are compared in Fig. 7 to the SANS structure factors, which were normalized by the Schulz form factor. Typically, it has been observed that using the HNC closure leads to a slightly higher charge as determined from the fit,[16] but that structures are very similar with predictable qualitative differences. Adding in some PY character to the solution will qualitatively increase the magnitude of the secondary and higher order maxima and minima, which would improve the correspondence to the data. These fits are similar in comparison to the data with previous SANS measurements on hard-sphere-like suspensions.[21] Some of the discrepancy in the first peak height can be attributed to loss of resolution in the signal by both the discrete detector array and the radial averaging. The fits were constructed to reproduce the low q data and fit the width of the first peak and the position of the second peak accurately. This results in overpredictions for the height of the first maximum, and underpredictions for the secondary and higher order peaks. It is our opinion that a full RY solution would thus be in better qualitative agreement with the measurements, but that the parameters determined would not vary significantly from those reported.

As shown in Fig. 3, some of our samples clearly exhibit multiphase behavior. It is possible that there also exists mixtures of liquid and glassy phases in some of the other concentrated samples. Indeed, this is also suggested by some of the rheological measurements, where multiple relaxation times are observed during frequency-dependent viscosity measurements.[40] A sample in this condition would exhibit structure factors that differ from a liquid in a manner qualitatively as we have observed here.

The results for the mean charge, and the salt concentration, are listed in Table V. The salt concentration determined in this manner is generally smaller than the value determined from Eq. (35). Titration measurements[39] yielded 1660 charges per particle, which is significantly larger than

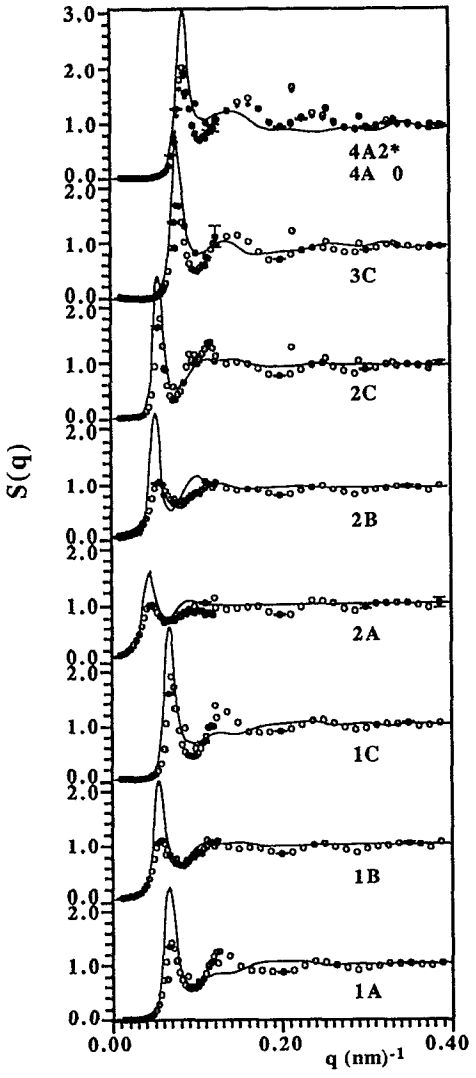

FIG. 7. $S(q)$ determined from SANS and the Schulz based form factors (O) and the model predictions (—).

that obtained by fitting the structure factor. This difference can result from a number of reasons, including that the titration measurements detect ions that may be weakly bound, and that the use of the linearized Debye–Hückel potential (Yukawa) for such highly charged and concentrated suspensions is an approximation. It is known that the true zeta potential will be higher (e.g., see Ref. 30) and so it is safest to view the charge determined by the fit of the structure factor as the effective charge applicable to this model. This fit nonetheless is a characteristic of the system that can be used in further studies of the dynamics.[15]

A comparison between the structure resulting from using the Schulz distribution and the TEM based distribution to fit the form factor is shown in Fig. 8 for sample 1C. The TEM based fit results in a lower first peak and a higher second peak, with a phase difference for the higher order peaks. In general, the Schulz distribution based fit was more satisfactory, but as shown, the differences are small. The general agreement among the radii determined by the Schulz distribution form factor fit, the Guinier plot, and DLS measurements encouraged the use of the Schulz model in the structure fits.

Figure 9 is a comparison of the above determined structure factors and form factors from the Schulz distribution against the actual scattering ratios, corrected by the Porod data for the background. As noted by previous investigators,[21] these are less discriminating than plots of $S(q)$, but they do show that many details of the overall fit are reasonably represented by our analysis.

The structures of the diluted samples with ion exchange resin, as determined by static light scattering, are shown in Fig. 10. Samples W1 and W4 were used for normalization and showed no significant structure. The structures shown are more similar to those measured for simple fluids, with sharper and higher first peaks. These samples have a Debye length that is many times the particle size, and hence size polydispersity does not play as important a role in influencing the structure as in the SANS samples, where the screening length is a fraction of the particle diameter.

The structures determined by QELS were fit by the integral theory using a three component discretization and the RY closure. The results of this best fit for the colloid charge and the concentration are shown in Fig. 10 and are tabulated in Table VI. The particle size and the polydispersity were

TABLE V. SANS fit results.

System	C_{salt} (mM)	Q_{HNC}	ϕ_{HNC}
1A	0.30	340	0.181
1B	0.38	420	0.11
1C	0.25	300	0.208
2A	0.29	390	0.06
2B	0.087	390	0.092
2C	0.010	340	0.119
3C	0.050	300	0.285
4A, 4A2	0.50	300	0.353

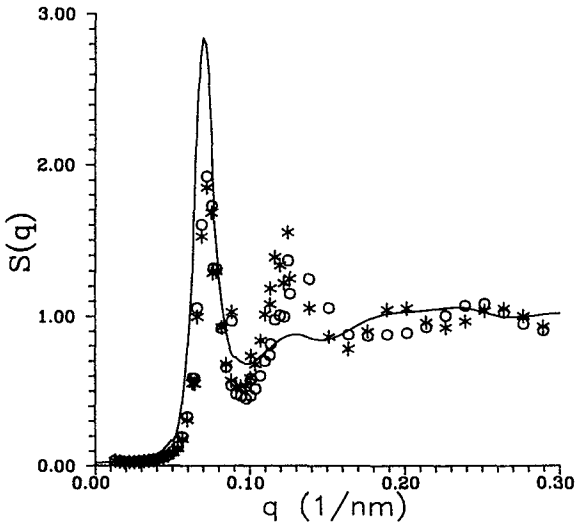

FIG. 8. Comparison of the $S(q)$ normalized with the Schulz form factor (O) and that from the TEM based distribution (*) for sample 3C; (-) model fit.

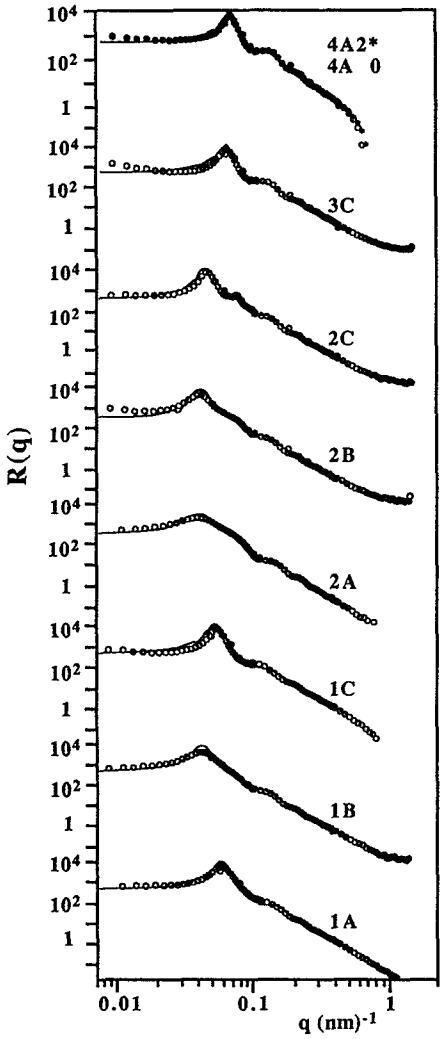

FIG. 9. SANS measured scattering ratio $R(q)$ (O) and model predictions (—).

taken from the neutron measurements (35 nm and 16%). The effective charge determined in this way is consistent with that from the SANS fits and is significantly lower than the titration results. Also given in Table VI are the charge and volume fraction determined by Monte Carlo simulation. This fit is not nearly of the same quality as that shown for the RY closure integral equation as the MC results are for a monodisperse suspension. Accounting for the polydispersity in size and charge is important in modeling these suspensions, as evidenced by the disparity between the charge determined from the MC simulation and the integral equation method. This is true even in those samples where the screening length is much longer than the radius of the particles due to polydispersity in charge.

For a suspension of spherical particles, the primary peak position should scale as $q_{\max} \approx 2\pi/\bar{d}$, where $\bar{d}$ is the mean spacing between the spheres. This spacing scales as the volume fraction to the minus one-third power $\bar{d} \propto \phi^{-1/3}$, with some proportionality constant that depends on the type of structure assumed for the packing. Shown in Fig. 11 is a plot of the primary peak position vs $\phi^{1/3}$ for all of the QELS and SANS structures. The best fit line through the origin has slope 0.12, which yields an estimate for $a \approx 30$ nm based on assuming random close packing, a value in good agreement with the measured values. Some of the scatter about the fit line in the SANS data is resultant from the finite size of the detector elements limiting the resolution of the peak position.

The value of both $S_{\text{eff}}(q=0)$, which is measured by the scattering, and $S(q=0)$, the true thermodynamic structure which is inversely proportional to the osmotic compressibility, can be extrapolated from the theoretical fits to the SANS data. The results from the model fits for $S(0)$ are given in Table VII. The SANS data are plotted as $\ln[1/S(q=0)]$ vs volume fraction in Fig. 12. The utility of this plot is it distinguishes readily the effects of screening length on the interparticle interaction, due to controlling the salt concentration. Theoretical results[56,57] and experimental data for hard-sphere systems have shown that such a plot yields a straight line over a wide range of volume fractions, with a slope that depends on the polydispersity of the sample, ranging from 7.90 downward slightly with increasing polydispersity. The SANS data roughly group as expected, with the outlying sample 1B having the greatest error bars associated with the fit, as it has the least structure.

An effective hard-sphere volume fraction for charged suspensions can be defined as[58]

$$\phi_{\text{eff}} = \phi\left(1 + \frac{\alpha}{\kappa a}\right)^3, \tag{36}$$

where κ is the inverse Debye screening length[31] and is given by the ionic strength of the solution. In the calculation of the inverse screening length, the particle charge and the salt concentration as determined by the model fits were used. Then it was assumed that each value of $\ln[1/S(0)]$ lies on a straight line through the origin. The ratio of the slope of this line to the hard-sphere value of 7.9 gives the ratio ϕ_{eff}/ϕ. Using the κa values calculated from the model fits results in values for the parameter α, as listed in Table VII. The results for α based on this approximation and earlier experiments on mapping the phase transition of charged colloidal systems similar to those studied here determined $\alpha \approx 1.64$, which is similar to values obtained by computer simulations.[58] This simple parametrization results in values within a factor of 2, but with no unique value for the entire sample set. Samples 4A and 3C exhibited strong viscoelastic behavior characteristic of a glassy solid, which might explain some of the difference in the α values between these samples and the more liquidlike SANS samples. The very dilute light scattering samples show a trend toward increasing α with particle concentration. It is also of interest that an analysis using the values of $S_{\text{eff}}(q=0)$ leads to similar results, except that the α values are slightly lower. This similarity is expected as the polydispersity is constant for all the samples. Using a lower value of the hard-sphere slope to account for polydispersity will increase the resultant values of α only slightly.

D. Dynamic light scattering results

Dynamic studies of the samples with structure were fit both with a short time polynomial fit and the complete dou-

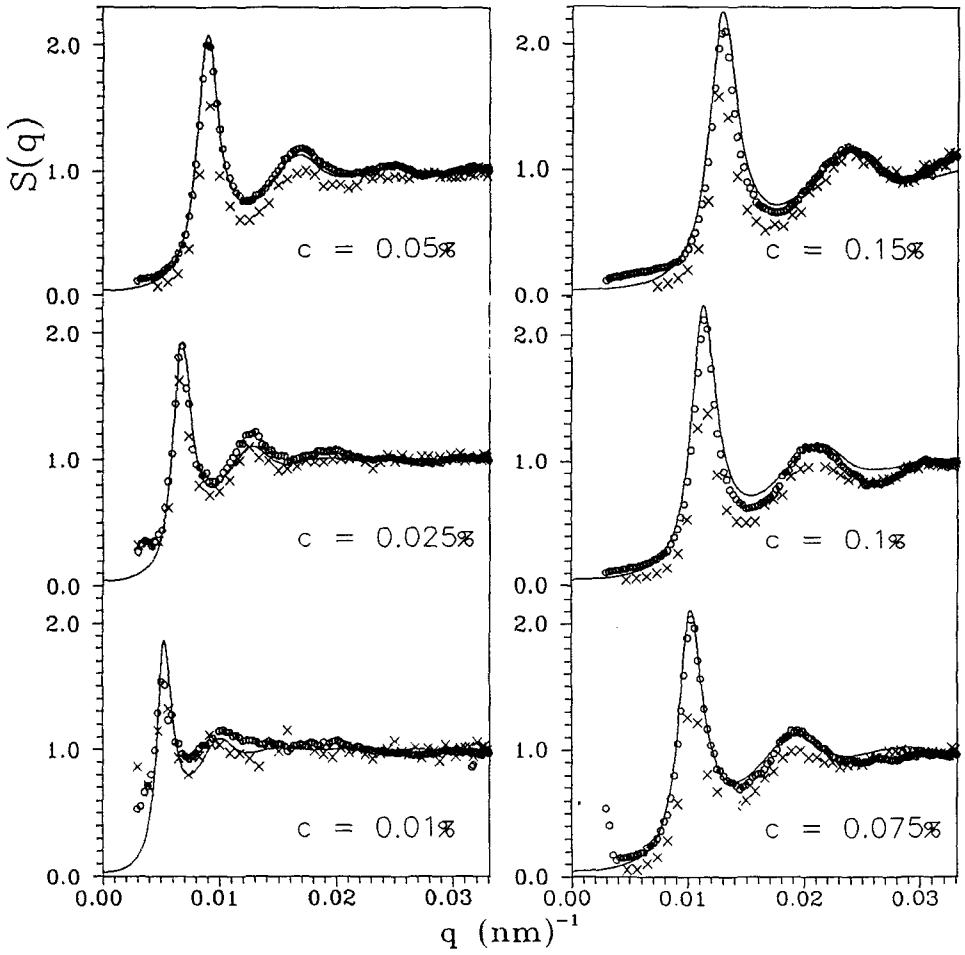

FIG. 10. $S(q)$ determined from QELS as compared to the theoretical fits. (OOO) static light scattering measurements; (×××) DLS $S(q)$ from the first cumulant; (—) OZ–RY theoretical fit.

ble exponential to extract the cumulants and the relaxation times. Typical time decays of the structure are well represented by the double exponential ansatz, as demonstrated in Fig. 13. We found essentially identical results for the first and second cumulants as determined by both methods. Shown in Figs. 14(a) and 14(b) are some representative results for the first and second cumulants. K_1 clearly reflects the underlying microstructure as characterized by $S(q)$. The second cumulant is very noisy and of lower magnitude than the first, although the shape of these functions resemble the corresponding first cumulants.

The results of reducing the first cumulant to $S(q)$ by assuming that $H(q) = 1$ and using relation (27) are also given in Fig. 10. The DLS structure is systematically lower than that obtained directly from static measurements in all

TABLE VI. QELS fit results.

System	ϕ	Q_{MC}	ϕ_{MC}	Q_{RY}	ϕ_{RY}
W2	0.0125%	210	0.0115%	390	0.01%
W3	0.025%	270	0.025%	390	0.0205%
W5	0.05%	270	0.055%	390	0.047%
W6	0.075%	255	0.085%	380	0.07%
W7	0.10%	265	0.12%	400	0.095%
W8	0.15%	260	0.17%	390	0.14%

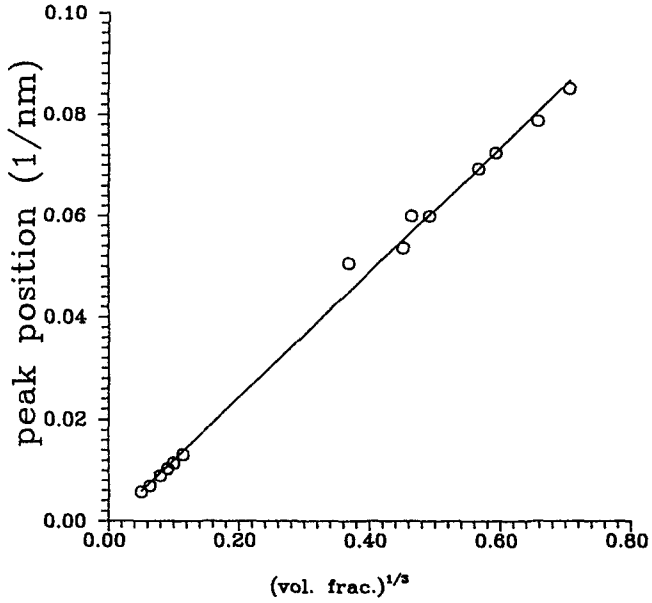

FIG. 11. Position of the maximum in $S(q)$ vs $\phi^{1/3}$ for QELS and SANS structures (O), (—) best fit line.

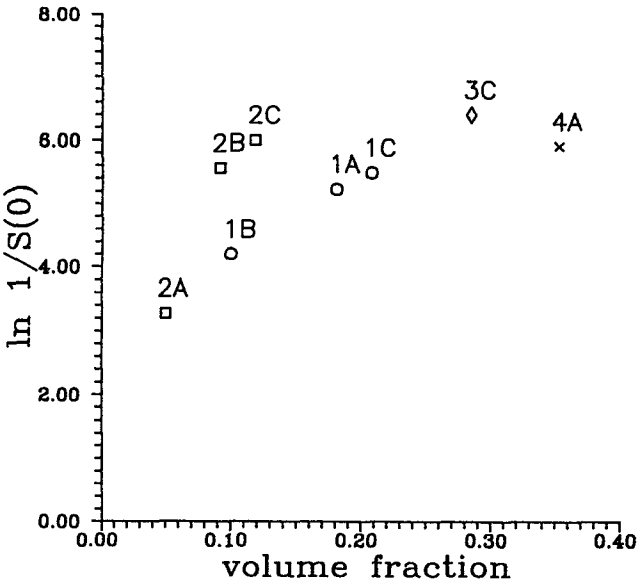

FIG. 12. ln $[1/S(0)]$ vs the volume fraction for the SANS samples.

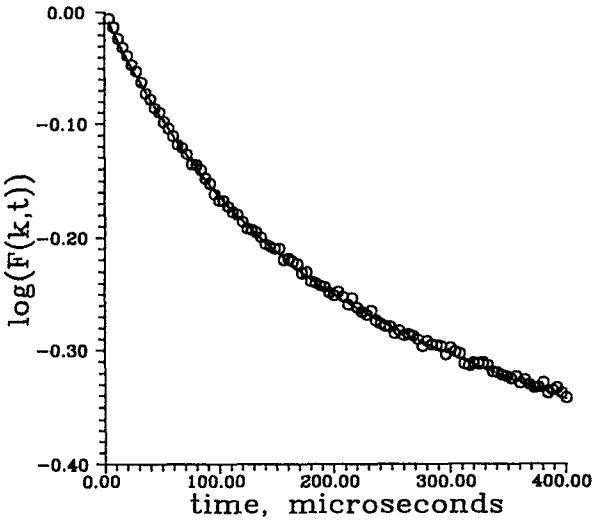

FIG. 13. Demonstration of the double exponential fit of the DLS data. (O) Data from sample W6 at 16°; (—) nonlinear least-square fit.

cases. This may be due to hydrodynamic interaction such that $H(q) > 1$, or that polydispersity effects in size and charge are significant. At these dilute concentrations, estimations of the increased hydrodynamic drag due to particle interaction are negligible. However, Eq. (27) is derived for a monodisperse suspension. Since the first cumulant is a dynamical quantity, it is a different moment of the size and charge distributions than the intensity of the light scattered from the particles. Thus, it is likely that this trend could be predicted by a more general derivation of this relation.

Typical time constants and the weighting factors determined from the double exponential fit of the dynamical measurements are given in Fig. 15. The dominant relaxation time, chosen to be $\tau_1(q)$, strongly reflects the underlying microstructure and is nearly the inverse of the first cumulant. As shown, $\tau_2(q)$ is very noisy and is two orders of mag-

TABLE VII. Effective hard-sphere parametrization.

System	ϕ	$S(q=0)\times 10^2$	κa	α
W2	0.01%	0.30	0.048	0.89
W3	0.0205%	0.32	0.069	0.99
W5	0.047%	0.34	0.11	1.1
W6	0.070%	0.34	0.13	1.2
W7	0.095%	0.37	0.15	1.3
W8	0.14%	0.35	0.18	1.3
1A	0.181	0.54	2.8	1.5
1B	0.10	1.5	2.8	2.1
1C	0.208	0.42	2.8	1.4
2A	0.05	3.8	1.6	1.6
2B	0.092	0.39	1.8	1.7
2C	0.119	0.25	1.6	1.4
3C	0.285	0.17	2.4	1.0
4A	0.353	0.28	3.7	1.0

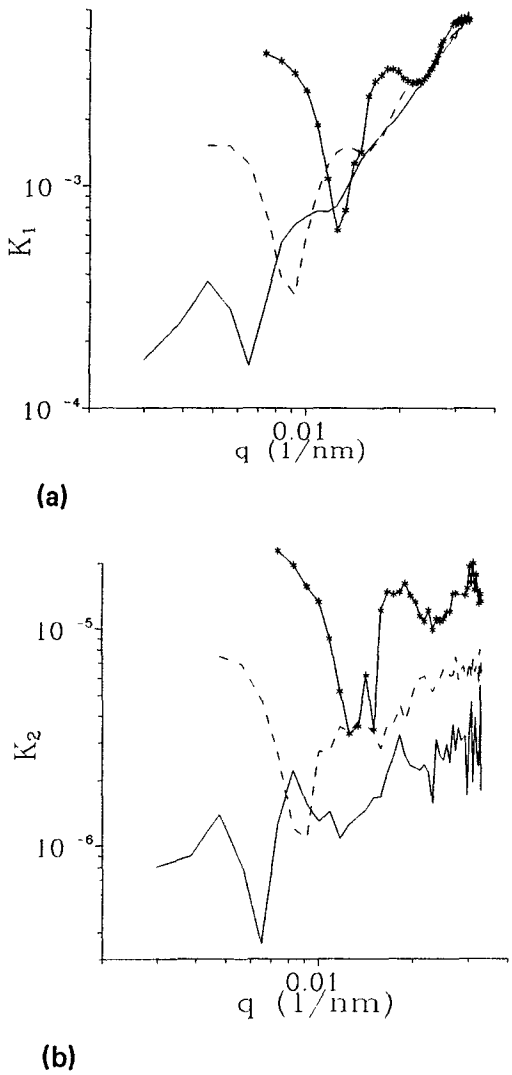

FIG. 14. (a) First K_1 and (b) second K_2 cumulants for three samples (—) W3; (- - -) W5; and (—*—*) W8.

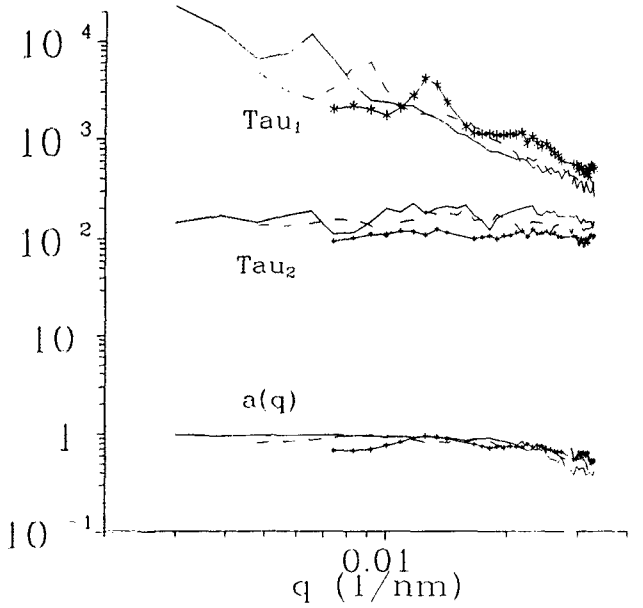

FIG. 15. Relaxation times $\tau_1(q)$ and $\tau_2(q)$ and the weighting function $a(q)$ for three samples (—) W3; (- - -) W5; and (—*—*) W8.

nitude lower than $\tau_1(q)$. It is also approximately constant over the entire range of q values probed. The weighting factor $a(q)$ again reflects some character of the underlying structure. These observations are predicted qualitatively by the mode coupling formalism that is based on the viscoelastic approximation.[7] For weakly viscoelastic systems, $\tau_1(q)$ and $a(q)$ can be related simply to the first and second cumulants, with small corrections that are related to $\tau_2(q)$.

V. CONCLUSIONS

Structure measurements of a model polydisperse suspension of charged colloids are reported over a wide range in both particle and added salt concentration. Comparisons of static QELS measurements with an integral equation for the structure, which accounts for both polydispersity in size and charge, are in good agreement and yield an effective surface charge of about 390e. Dynamic QELS measurements yield a structure factor from analysis of the first cumulant that is consistently lower than the static measurements. This discrepancy is postulated to be an effect of the polydispersity in size and charge on the particles. The cumulants determined from a double exponential fit of the relaxation of the intensity autocorrelation function are in excellent agreement with those determined from a short time polynomial fit. The viscoelastic relaxation times determined from the double exponential fit show a primary q-dependent relaxation time that is essentially the inverse of the first cumulant, and a secondary relaxation time that is significantly smaller and less important in weighting.

SANS measurements of the structure of concentrated samples spanning the liquid to glass regimes, for which extensive rheological measurements have been made, are reported. A Schulz model for the particle size distribution fit to the dilute SANS measurements yielded $\bar{a} = 35.0$ nm with 16% polydispersity. Guinier and Porod analysis of the SANS measurements and DLS results demonstrate the consistency of the data. The resultant SANS structures show some qualitative differences in shape to those measured in the dilute samples by QELS and to predictions of the integral equation theory, including lower primary peaks and higher secondary peaks. Comparison with the HNC solutions of the integral equation theory yield good agreement for the low q data, the primary peak width, and the secondary peak position, with a discrepancy in the primary peak height. This may be partially attributable to losses in resolution, the use of the HNC closure, and the possibility of multiple phases. The primary peak positions fit on the same line as the QELS data when plotted against $\phi^{1/3}$. An effective hard-sphere parametrization based on the osmotic compressibility resulted in an α value that varied by a factor of 2 with a deterministic dependence on particle concentration. The salt concentration determined from the fit is generally lower than that predicted by the Donnan equilibrium and the mean surface charge is significantly lower than reported by titration measurements, but in good agreement with that measured by QELS. The integral equation theory is able to fit the data for these polydisperse, charged suspensions from the dilute to strongly correlated liquid regimes, providing a parametrization for use in further structural studies.

In future work, we intend to use these measured structures and system parameters to quantitatively test various statistical mechanical theories relating the structure of complex fluids to their measured rheological behavior.

ACKNOWLEDGMENTS

The authors would like to thank Dr. S. Keeping (Bristol University) for supplying the colloids used in this investigation. N.J.W. acknowledges the support of a postdoctoral fellowship through Los Alamos National Laboratory and thanks Professor R. Klein for useful discussions. The support of the Deutsche Forschungsgemeinschaft is also gratefully acknowledged.

[1] G. K. Batchelor and J. T. Green, J. Fluid. Mech. **56**, 375 (1972); **56**, 401 (1972).
[2] G. K. Batchelor, J. Fluid Mech. **74**, 1 (1976).
[3] G. K. Batchelor, J. Fluid Mech. **83**, 97 (1977).
[4] T. Ohtsuki, Physica A **108**, 441 (1981).
[5] T. Ohtsuki, Physica A **122**, 212 (1983).
[6] R. Klein and W. Hess, Faraday Discuss. Chem. Soc. **76**, 137 (1983).
[7] W. Hess and R. Klein, Adv. Phys. **33**, **173** (1983).
[8] R. Klein, W. Hess, and G. Naegele, *Physics of Complex and Supermolecular Fluids*, edited by S. A. Safran and N. A. Clark (Wiley, New York, 1987), p. 67.
[9] B. U. Felderhof and R. B. Jones, Physica A **146**, 417 (1987).
[10] J. K. G. Dhont, Physica A **146**, 541 (1987).
[11] B. U. Felderhof, Physica A **147**, 203 (1987); **147**, 533 (1987).
[12] W. B. Russel and A. P. Gast, J. Chem. Phys. **89**, 1580 (1988).
[13] N. J. Wagner and W. B. Russel, Physica A **155**, 475 (1989).
[14] J. K. G. Dhont, J. Fluid Mech. **204**, 421 (1989).
[15] N. J. Wagner and R. Klein, Colloid Polymer Sci. (to be published).
[16] B. D'Aguanno and R. Klein, J. Chem. Soc. Faraday Trans. **87**, 379 (1991).
[17] N. J. Wagner, G. G. Fuller, and W. B. Russel, J. Chem. Phys. **89**, 1580 (1988).

[18] R. L. Hoffmann, Trans. Soc. Rheol. **16**, 155 (1972).
[19] R. L. Hoffmann, J. Chem. Phys. **46**, 491 (1974).
[20] C. G. deKruif, E. M. F. van Iersel, A. Vrij, and W. B. Russel, J. Chem. Phys. **83**, 4717 (1985).
[21] C. G. deKruif, W. J. Briels, R. P. May, and A. Vrij, Langmuir **4**, 668 (1988).
[22] B. J. Ackerson, J. van der Werff, and C. G. de Kruif, Phys. Rev. A **37**, 4819 (1988).
[23] B. J. Ackerson, C. G. de Kruif, N. J. Wagner, and W. B. Russel, J. Chem. Phys. **60**, 3250 (1989).
[24] S. J. Johnson, C. G. de Kruif, and R. P. May, J. Chem. Phys. **89**, 5909 (1988).
[25] J. C. van der Werff, Ph.D. thesis, Rijksuniversiteit te Utrecht, 1990.
[26] N. J. Wagner and W. B. Russel, Phys. Fluids **2**, 491 (1990).
[27] J. C. van der Werff, B. J. Ackerson, R. P. May, and C. G. de Kruif, Phys. Status Solidi A **165**, 375 (1990).
[28] J. F. Brady and G. Bossis, Annu. Rev. Fluid Mech. **20**, 111 (1988).
[29] G. Bossis and J. F. Brady, J. Chem. Phys. **91**, 1866 (1989).
[30] S. Bell, G. M. Levine, and L. N. McCartney, J. Colloid Interface Sci. **33**, 335 (1970).
[31] P. Hiemenz, *Principles of Colloid and Surface Chemistry*, 2nd ed. (Marcel Dekker, New York, 1986).
[32] W. B. Russel, *The Dynamics of Colloidal Systems* (University of Wisconsin, Madison, Wis., 1987).
[33] B. J. Ackerson and N. A. Clark, Phys. Rev. A **30**, 906 (1984).
[34] W. B. Russel, J. Fluid Mech. **85**, 209 (1985).
[35] H. M. Lindsay, W. D. Dozier, P. M. Chaiken, R. Klein, and W. Hess, J. Phys. A: Math Gen. **19**, 2583 (1986).
[36] S. Ashdown, I. Markovic, R. H. Ottewill, P. Lindner, R. C. Oberthur, and A. R. Rennie, Langmuir **6**, 303 (1990).
[37] D. J. Cebula, J. W. Goodwin, G. C. Jeffrey, R. H. Ottewill, A. Parentich, and R. A. Richardson, Faraday Discuss. Chem. Soc. **76**, 37 (1983).
[38] R. H. Ottewill and A. R. Rennie, Int. J. Multiphase Flow **16**, 681 (1990).
[39] S. Keeping, Ph.D. thesis, University of Bristol, 1989.
[40] J. Goodwin and S. Keeping, Langmuir (to be published).
[41] J. B. Hayter, *Physics of Amphiphiles: Micelles, Vesicles, and Microemulsions*, edited by V. Degiorgio and M. Corti (North-Holland, Amsterdam, 1985), p. 59.
[42] H. C. van de Hulst, *Light Scattering by Small Particles* (Dover, New York, 1957).
[43] *Guide to Neutron Research Facilities at the ILL*, edited by H. Blank and B. Maier (Institute Laue-Langevin, Grenoble, France, 1988).
[44] A. Guinier and G. Fournet, *Small Angle Scattering of X Rays* (Wiley, New York, 1955).
[45] K. Ibel, J. Appl. Crystallogr. **9**, 296 (1976).
[46] J. B. Berne and R. Pecora, *Dynamic Light Scattering* (Wiley, New York, 1976).
[47] B. J. Ackerson, J. Chem. Phys. **64**, 242 (1976).
[48] B. J. Ackerson, J. Chem. Phys. **69**, 684 (1978).
[49] R. E. Ghosh, *A Computing Guide for Small Angle Scattering Experiments* (Institute Laue-Langevin, Grenoble, France, 1989).
[50] W. H. Press, B. P. Flannery, S. A. Teukolsky, and W. T. Vetterling, *Numerical Recipes* (Cambridge University, Cambridge, 1986).
[51] J. P. Hansen and I. R. McDonald, *Theory of Simple Liquids* (Academic, London, 1986).
[52] W. van Megen and I. Snook, J. Chem. Phys. **66**, 813 (1977).
[53] D. A. McQuarrie, *Statistical Mechanics* (Harper and Row, New York, 1976).
[54] F. J. Rogers and D. A. Young, Phys. Rev. A **30**, 999 (1984).
[55] P. W. Atkins, *Physical Chemistry*, 2nd ed. (Freeman, San Francisco, 1982), pp. 812 ff.
[56] A. Vrij, J. Colloid Interface Sci. **90**, 110 (1982).
[57] A. Vrij, J. W. Jansen, J. K. G. Dhont, C. Pathmamanoharan, M. M. Kops-Werkhoven, and H. M. Fijnaut, Faraday Discuss. Chem. Soc. **7**, 19 (1983).
[58] S. Mitaku, T. Ohtsuki, A. Koshimoto, and K. Okano, Biophys. Chem. **11**, 411 (1980).